PHYSICAL REVIEW B VOLUME 22, NUMBER 4 15 AUGUST 1980

Linear-combination-of-atomic-orbitals–coherent-potential-approximation studies of carbon vacancies in the substoichiometric refractory monocarbides NbC_x, TaC_x, and HfC_x

B. M. Klein, D. A. Papaconstantopoulos, and L. L. Boyer
Naval Research Laboratory, Washington, D.C. 20375
(Received 7 February 1980)

We have calculated the electronic densities of states and Bloch spectral functions of the refractory monocarbides NbC_x, TaC_x, and HfC_x, $0.7 \leq x \leq 1.0$, using the coherent-potential approximation in a linear-combination-of-atomic-orbitals (LCAO) basis. The LCAO Hamiltonian is derived from self-consistent augmented-plane-wave calculations performed for the stoichiometric materials, $x = 1.0$. We discuss the bonding and charge transfer in these compounds and show that the latter is crucial for interpreting the Fermi-level motion of the substoichiometric materials. In all cases the charge transfer is from the transition metal to carbon. We present results of the smearing of the Fermi surfaces for $x < 1.0$ due to lifetime broadening of the electron quasiparticles, and we argue that the superconducting and phononic properties are greatly affected by this. Further comparisons are made between our results and Hall-effect, resistivity, specific-heat, and photoelectron-spectra measurements.

I. INTRODUCTION

The refractory transition-metal carbides have many unusual and interesting properties which have attracted a number of experimental and theoretical investigations. A monograph by Toth[1] gives an excellent general discussion of the carbides and is a good literature source up to approximately 1970. The carbides are renowned for their great hardness and high melting temperatures, properties which lend themselves to important applications as structural materials or as cutting tools. Strong metal-carbon covalent-like bonding is usually assigned as the underlying mechanism. Even though this type of bonding is usually ascribed to nonmetallic materials, nearly stoichiometric carbides are often good metallic conductors with conductivities having values similar to those of the parent transition metals. Furthermore, several of the carbides with nine valence electrons per molecule (e.g., NbC and TaC) are found to be superconductors with transition temperatures $T_c \sim 11$ K at stoichiometry, several degrees higher than metallic Nb and Ta. On the other hand the 8-valence-electron-per-molecule carbides (e.g., ZrC and HfC) do not superconduct and are characterized by relatively poor conductivities and generally weaker metallic properties. Klein and Papaconstantopoulos[2] have done calculations of the superconducting properties of the stoichiometric carbides and have given a qualitative discussion of the relationship between T_c and the electronic structure.

Smith and Gläser's[3] discovery of phonon anomalies or dips in the phonon-dispersion curves for NbC and TaC but not for HfC or ZrC brought forth an interesting correlation between phonon instabilities and superconductivity in these compounds. Weber *et al.*[4] and Weber[5] did theoretical calculations of the phonons in these materials and found that the anomalies could be related to a "... resonance-like increase of the electronic polarizability ..." due to the transition-metal d electrons. Subsequent theoretical work by Gupta and Freeman,[6] and by Klein *et al.*[7,8] showed that this resonance might be related to enhanced electron-phonon scattering across the nested jungle-gym Fermi surfaces of NbC and TaC. These nesting features (and the phonon anomalies) are absent in HfC and ZrC (Refs. 6–8). Unfortunately the lack of good stoichiometric single-crystals of the carbides has so far precluded observing the Fermi surfaces by conventional de Haas-van Alphen techniques. In fact it is a well-known characteristic of the carbides that they tend to form with significant amounts of carbon vacancies, usually 1% or more.[1] This situation provided one of the motivations for the present work—to perform electronic-structure calculations for the substoichiometric carbides to determine the changes in, among other quantities, the Fermi surfaces when carbon vacancies are present. The theoretical results could then be compared with positron annihilation or Compton scattering measurements on substoichiometric carbides. We hope that the availability of the theoretical information to be described will stimulate such experiments.

In this paper we present the results of studies of the electronic structures of substoichiometric NbC_x, TaC_x, and HfC_x, $x \leq 1.0$. The calculations have been done using the coherent-potential approximation (CPA) in a linear-combination-of-atomic-orbitals (LCAO) basis determined by fitting to self-consistent augmented-plane-wave (APW)

calculations. We refer to the procedure as the LCAO–CPA method. The formalism we use closely follows the work of Faulkner[9] with some additional complications to be described. We have considered the crystal sites to consist of those of the stoichiometric sodium chloride structure, with the fcc transition-metal (M) sites fully occupied, and the fcc carbon sites randomly occupied with probability x. In the range that we have studied, $0.7 \leq x \leq 1.0$, this appears to be a good representation of the substoichiometry.[1] Also since the lattice-constant variations in this range of x are relatively small (~1%), this effect is neglected in our LCAO–CPA calculations. Faulkner's[9] original formulation was designed to treat hydrogen vacancies in PdH_x, and it was only necessary to consider s-like electrons of the vacancy atoms in that case. For the carbides, the occupied valence states of the carbon atoms contain both s and p electrons so that some relatively straightforward modifications to Faulkner's[9] method are needed. In effect one has to solve the Green-function equations self-consistently for two different self-energies corresponding to the carbon s and p electrons.

Klima[10] has recently done LCAO–CPA calculations for TiC using Faulkner's method with some approximations to the LCAO Hamiltonian beyond the ones we make. In addition Klima neglects the s self-energy of carbon, arguing that for the upper valence and conduction-band states there is very little admixture of carbon s states. Although this may be a fairly good approximation, we recommend avoiding it since including both the s and p self-energies is rather straightforward. We further note a new aspect in our work. We place a large emphasis on the calculated charge transfer in the carbides ($M \rightarrow C$) in interpreting our numerical results and putting together a physical model of their behavior. This interpretation is absent in Klima's work.

The present paper is organized into eleven sections. In Sec. II we discuss the APW band-structure techniques used for the stoichiometric-crystal calculations; in Sec. III we show how the LCAO Hamiltonian used in the CPA is generated. Section IV details the CPA methodology and the numerical methods used to solve for the self-energies, densities of states, etc. Band structures, densities of states, and Fermi surfaces of the stoichiometric materials are presented in Sec. V and compared with other works. The CPA numerical results are presented in Sec. VI, and charge-transfer, bonding, and the Fermi-surface changes induced by carbon vacancies are discussed. In Secs. VII and VIII we discuss the phonon anomalies and superconducting properties of the carbides in the context of our LCAO–CPA results. In Sec. IX we show the results of broadened densities of states as a function of x, and compare with available photoelectron-spectra measurements. Comparisons with Hall-effect, resistivity, and specific-heat measurements are made in Sec. X. Finally a summary of the major conclusions drawn from this work are made in Sec. XI.

II. APW BAND-STRUCTURE METHODOLOGY

Most of the APW band-structure procedures that we used are fully documented in the review articles by Mattheiss *et al.*,[11] and by Dimmock,[12] so that here we limit ourselves to describing some of the details pertinent to our self-consistent (SC) procedures. At the end of this section we will also describe the procedures used to calculate the stoichiometric densities of states.

The APW calculations were done in the muffin-tin approximation with lattice constants of 8.4206, 8.7683, and 8.4471 a.u., for TaC, HfC, and NbC, respectively. The crystal structure is B1 or sodium chloride. For Nb and C the $X\alpha$ exchange approximation was used, with the α values obtained from the work of Schwarz[13]; while for Ta and Hf a value of $\alpha = \frac{2}{3}$ was used. In the interstitial region we used $\alpha = \frac{2}{3}$. Warped muffin-tin corrections (removing the approximation of constant interstitial charge density and potential) were not included, but these are expected to be small based on the results of Herzig[14] and of Trebin and Bross[15] for isostructural TiC. The bonding in TiC and NbC, TaC, and HfC are known to be quite similar.

Relativistic effects, neglecting spin-orbit coupling, were included following the method of Mattheiss.[16] In this procedure the spin-orbit term is dropped from the APW matrix elements but all other relativistic terms are explicitly included in the SC cycles.[17] We note that subsequent to these calculations we have verified that, except for bands close to logarithmic derivative asymptotes (well above the Fermi energy), Mattheiss' method[16] and the somewhat different relativistic approach of Koelling and Harmon[18] give nearly identical results (usually the same within the convergence accuracy of our APW basis). By comparing our semirelativistic NbC band calculations with our unpublished nonrelativistic calculation for the same material and with the work of Schwarz,[19] we conclude that relativistic corrections, especially for HfC and TaC, lead to shifts in relative band energies of 10 mRy or more. Relativistic corrections thus are nontrivial, especially regarding details of the density of states and Fermi surface. Weinberger *et al.*[20] have also noted the importance of relativistic corrections

for TaC and HfC.

In our calculations the states treated as bands were: Nb($4s$, $4p$, $4d$, $5s$), Ta($5s$, $5p$, $5d$, $6s$), Hf($5s$, $5p$, $5d$, $6s$), and C($2s$, $2p$). For the calculations reported here, the inner core-state charge densities were kept fixed ("frozen-core" approximation) in the course of the SC-APW iterations. A "soft-core" calculation was done separately for NbC subsequent to our original calculations, and we found relative shifts in valence-conduction eigenvalues of ~3 mRy. In light of this small change we decided not to redo TaC and HfC with a soft-core approach. Of course, a soft-core approximation would be necessary for an accurate total-energy calculation. Finally we note that the Hf and Ta $4f$ states which lie in the lower valence-band region were treated as core states due to their extremely small $\vec{k}$-space dispersion.

Starting potentials for the SC procedure were generated by forming superpositions of atomic radial-charge densities from the relativistic Hartree-Fock-Slater atomic-structure code of Liberman *et al.*[21] using the above-mentioned exchange approximations. Both the starting and all subsequent potentials were generated[22] from the charge densities by solving Poisson's equation within the muffin tins, with the interstitial constant potential calculated using the Ewald method. In the SC iterations newly generated APW charge densities were mixed with the charge density from the previous cycle (25% new with 75% old) to avoid numerical instabilities. Typically six or seven SC cycles were needed to converge the energy eigenvalues to ±3 mRy.

The muffin-tin radii were chosen by the condition of matching M and C potentials at the touching points of the spheres. In each SC cycle the radius ratios were varied until this condition was satisfied.

For the SC cycles we used a mesh of 6 $\vec{k}$ points: $\Gamma(000)$, $\Delta(010)$, $X(020)$, $\Sigma(110)$, $W(120)$, and $L(111)$, all in units of π/a. These six points in the $\frac{1}{48}$th irreducible Brillouin zone (IBZ) correspond to 32 $\vec{k}$ points in the full zone. Our experience with fcc-structure materials has shown us that this mesh is sufficient for good eigenvalue convergence.

In order to calculate the stoichiometric densities of states we make use of a two-step procedure. The LCAO Hamiltonian (see Sec. III) is used to calculate eigenvalues and eigenfunctions on a uniform mesh in the fcc IBZ, and the results are then integrated using the tetrahedral method[23] to form the densities of states $n(E)$ and $n_l^j(E)$. Here l are the angular momentum irreducible representations and j are the site indices. Their values are $l=\Gamma_1(s)$, $\Gamma_{15}(p)$, $\Gamma_{12}(d-E_g)$, and $\Gamma'_{25}(d-T_{2g})$; and $j=1$ (Nb, Ta, Hf) and $j=2$ (C). Our explicit $n(E)$ calculations to be shown were done for a mesh of 505 $\vec{k}$ points in the fcc IBZ. By comparing similar results on a mesh of 89 $\vec{k}$ points, we estimate the convergence accuracy of our densities of states to be ~1% at E_F.

III. LCAO FITTING PROCEDURE

The basic LCAO approach that we have used follows the method of Slater and Koster[24] with the multicenter integrals treated as parameters determined by a least-squares-fitting procedure using the APW eigenvalues. We have used a basis set of 13 wave functions: $s(1)$, $p(3)$, and $d(5)$ for the transition metals, and $s(1)$ and $p(3)$ for carbon. A total of 51 interaction integrals, up to second neighbors of the same kind of atom were included, with the overlap matrix set equal to unity. The LCAO parameters are listed in Table I.

The fitting procedure used 164 APW energy values from a mesh of 20 $\vec{k}$ points in the IBZ. This corresponds to at least nine bands for every $\vec{k}$ point; and, in addition, points from even higher bands were included in order to obtain parameters giving the correct wave-function character. This latter point, discussed in one of our previous papers on PdH,[25] arises because both atoms in these NaCl-structure compounds contain valence conduction-band states with s and p character (e.g., there are two Γ_1's and two Γ_{15}'s fairly close to E_F). To get the correct hybridization, the bonding and antibonding states must be included in the fit. Great care must be taken in this regard.

The LCAO Hamiltonian was symmetry reduced at each $\vec{k}$ point, and the least-squares fit was performed using a subroutine which does not require the evaluation of derivatives. The rms fitting accuracy was ~10 mRy for bands near E_F for NbC and TaC, slightly worse for the higher conduction and lower valence-band states. Maximum errors of ~30–40 mRy occurred for a few points 0.5 Ry or more away from E_F in these materials. In general the LCAO energy bands and Fermi surfaces, to be discussed, appeared nearly identical to our APW results. The largest errors in the HfC valence-band region occurred for states near E_F leading to somewhat larger discrepancies for $n(E_F)$ for this material compared with the APW-derived equivalents (see Sec. V). None of the conclusions in this paper are sensitive to this discrepancy.

IV. CPA THEORY AND NUMERICAL PROCEDURES

The tight-binding CPA approach that we have used follows the theory developed by Faulkner[9]

TABLE I. LCAO (Slater-Koster) parameters for NbC, TaC, and HfC. The entries are in Ry and the notation follows that of Ref. 24. ($d_1 = x^2 - y^2$; $d_2 = 3z^2 - r^2$.)

	NbC	TaC	HfC		NbC	TaC	HfC
			Metal-metal interactions				
$E_{s_1,s_1}(000)$	1.2461	1.1853	1.1852	$E_{x_1,xy}(020)$	0.0042	0.0150	0.0163
$E_{s_1,s_1}(110)$	−0.0424	−0.0338	−0.0380	$E_{z_1,d_2}(011)$	−0.0281	−0.0295	−0.0273
$E_{s_1,s_1}(200)$	0.0243	0.0074	0.0019	$E_{z_1,d_1}(011)$	−0.0149	−0.0139	−0.0069
$E_{s_1,x_1}(110)$	−0.0311	−0.0384	−0.0464	$E_{z_1,d_2}(002)$	0.0836	0.0865	0.0832
$E_{s_1,x_1}(200)$	0.0266	0.0218	0.0137	$E_{xy,xy}(000)$	0.9498	0.9842	1.0135
$E_{s_1,xy}(110)$	−0.0169	−0.0193	−0.0180	$E_{xy,xy}(110)$	−0.0612	−0.0678	−0.0698
$E_{s_1,d_2}(110)$	−0.0121	−0.0065	0.0036	$E_{xy,xy}(011)$	0.0162	0.0173	0.0166
$E_{s_1,d_2}(002)$	0.0480	0.0464	0.0380	$E_{xy,xy}(200)$	−0.0138	−0.0125	−0.0093
$E_{x_1,x_1}(000)$	2.6895	2.7690	2.6060	$E_{xy,xy}(002)$	0.0014	0.0029	0.0056
$E_{x_1,x_1}(110)$	−0.0387	−0.0437	−0.0505	$E_{xy,yz}(011)$	0.0028	0.0059	0.0093
$E_{x_1,x_1}(011)$	0.0340	0.0345	0.0140	$E_{xy,d_2}(110)$	0.0171	0.0195	0.0248
$E_{x_1,x_1}(200)$	0.2861	0.2850	0.2800	$E_{d_2,d_2}(000)$	0.9851	1.0311	1.0457
$E_{y_1,y_1}(200)$	−0.1270	−0.1255	−0.0917	$E_{d_2,d_2}(110)$	0.0048	0.0038	0.0000
$E_{x_1,y_1}(110)$	0.1958	0.2026	0.1865	$E_{d_1,d_1}(110)$	−0.0407	−0.0419	−0.0329
$E_{x_1,xy}(110)$	0.0300	0.0242	0.0393	$E_{d_2,d_2}(002)$	0.0603	0.0625	0.0613
$E_{x_1,xy}(011)$	0.0132	0.0115	0.0013	$E_{d_1,d_1}(002)$	−0.0069	−0.0061	−0.0050
	Carbon-carbon interactions				Metal-carbon interactions		
$E_{s_2,s_2}(000)$	0.1720	0.1689	0.1349	$E_{s_1,s_2}(100)$	0.1195	0.1205	0.1093
$E_{s_2,s_2}(110)$	0.0215	0.0177	0.0178	$E_{s_1,x_2}(100)$	−0.1815	−0.2070	−0.1914
$E_{s_2,s_2}(200)$	−0.0151	−0.0162	−0.0191	$E_{x_1,s_2}(100)$	0.1080	0.1084	0.1292
$E_{s_2,x_2}(110)$	−0.0287	−0.0281	−0.0256	$E_{x_1,x_2}(100)$	0.2645	0.2760	0.2717
$E_{s_2,x_2}(200)$	0.0439	0.0443	0.0436	$E_{y_1,y_2}(100)$	0.0138	0.0119	0.0060
$E_{x_2,x_2}(000)$	0.9949	1.0432	0.9724	$E_{xy,x_2}(010)$	0.0986	0.1035	0.0993
$E_{x_2,x_2}(110)$	0.0226	0.0249	0.0222	$E_{d_2,s_2}(001)$	−0.0208	−0.0250	−0.0138
$E_{x_2,x_2}(011)$	−0.0086	−0.0101	−0.0073	$E_{d_2,z_2}(001)$	−0.1790	−0.1921	−0.1939
$E_{x_2,x_2}(200)$	−0.0930	−0.1048	−0.0987				
$E_{y_2,y_2}(200)$	0.0098	0.0103	0.0064				
$E_{x_2,y_2}(110)$	0.0135	0.0115	0.0164				

extended to include both s and p orbitals in the LCAO basis set of the vacancy atom. We refer the reader to Faulkner's paper[9] for details of the formalism, and here we will show mainly the modifications to the theory needed to treat the carbide systems.

We define the Green-function matrix of the stoichiometric system

$$\underline{g}(\vec{k}, E) \equiv [\underline{z}^+ - \underline{H}(\vec{k})]^{-1}, \tag{1}$$

where

$$\underline{z}^+ \equiv (E + i\delta)\underline{I}, \tag{2}$$

δ is a small positive number ($\delta \to 0^+$ is implied), $\underline{I}$ is the unit matrix, and $\underline{H}(\vec{k})$ is the 13×13 LCAO Hamiltonian matrix. As noted in Sec. III we have not included wave-function overlap parameters in our LCAO approach so that the overlap matrix is $\underline{I}$.

If randomly distributed carbon vacancies are present with concentration $1-x$ [$1.0 \geq (1-x) \geq 0$ and $x = 1.0$ is full stoichiometry] the Green function of the system is

$$\underline{g}^x(\vec{k}, E) = [\underline{z}^+ - \underline{H}^x(\vec{k}, E)]^{-1}. \tag{3}$$

Here $\underline{H}^x(\vec{k}, E)$ is identical to $\underline{H}(\vec{k})$, except that the carbon-carbon $E_{\alpha,\alpha}(000)$ parameters (see Table I) are replaced by complex self-energies $\Sigma_s(E)$ and $\Sigma_p(E)$, to be determined below. The reader should keep in mind that in our notation $\underline{E}$ refers to the LCAO parameters while scalar E is the energy variable.

Defining the Brillouin-zone averaged Green function by

$$\underline{G}^x(E) \equiv \frac{1}{\Omega} \int \underline{g}^x(\vec{k}, E) d^3k, \tag{4}$$

a straightforward extension of Faulkner's theory[9,26] yields the equation for the self-energy:

$$\Sigma_s = E_{s,s}(000) - (1-x)/G^x_{10,10}(E), \tag{5}$$

$$\Sigma_p = E_{p,p}(000) - (1-x)/G^x_{11,11}(E). \tag{6}$$

Of course since $\underline{G}^x(E)$ contain both Σ_s and Σ_p, Eqs. (5) and (6) must be solved by iteration (see below). Note that there is only one independent p self-energy owing to cubic symmetry, and that

for the same reason $G^x_{11,11}(E) = G^x_{12,12}(E) = G^x_{13,13}(E)$. Having determined $\underline{G}^x(E)$, the density of states and the Bloch spectral functions are given by:

$$A(\vec{k}, E)_i \equiv -(1/\pi)\,\mathrm{Im}G^x(\vec{k}, E)_{i,i}\,, \tag{7}$$

$$n_i(E) = \frac{1}{\Omega}\int A_i(\vec{k}, E)d^3k\,, \tag{8}$$

$$n(E) = \sum_{i=1}^{13} n_i(E) = -\frac{1}{\pi}\,\mathrm{Im\,Tr}\underline{G}^x(E)\,. \tag{9}$$

In the notation of Eq. (9) the partial densities of states are

$$\begin{aligned}
&n_s^M(E) = n_1(E)\,,\\
&n_p^M(E) = n_2(E) + n_3(E) + n_4(E)\,,\\
&n_{d-T_{2g}}^M(E) = n_5(E) + n_6(E) + n_7(E)\,,\\
&n_{d-E_g}^M(E) = n_8(E) + n_9(E)\,,\\
&n_s^C(E) = n_{10}(E)\,,\\
&n_p^C(E) = n_{11}(E) + n_{12}(E) + n_{13}(E)\,,
\end{aligned} \tag{10}$$

where the basis set has been ordered 1–13 in an obvious manner.

The spectral function $\sum_i A_i(E)$ will be discussed in Sec. VI and will be shown to give useful information regarding changes in the Fermi surfaces of the substoichiometric carbides.

By using straightforward group-theoretical techniques the integrals in Eq. (4) may be restricted to the IBZ. All of these integrals were performed by evaluating the integrands on a uniform mesh of 356 $\vec{k}$ points in the IBZ, using linear tetrahedral interpolation[23] to expand onto a mesh of 4495 points, and then summing the properly weighted contributions.

The limits $\delta \to 0+$ presents some numerical difficulties. As one approaches the case $x \to 1.0$, Σ_s and Σ_p become real, and the imaginary part of $\underline{G}^x(\vec{k}, E)$ becomes a delta function at each eigenvalue location. Convergence (in $\vec{k}$ space) of the integrals becomes extremely difficult. In practice one chooses a small but finite value of δ, in our case 0.001 Ry, and refines the $\vec{k}$ mesh until adequate stability is obtained. In the same process the energy-sampling mesh is refined to obtain a sufficiently accurate Fermi energy. Proceeding off stoichiometry, both Σ_s and Σ_p develop imaginary components which help stabilize the whole numerical procedure. For $x \leq 0.9$ good stability is obtained, and the resultant density of states has very little "noise."

The SC procedure for determining $\Sigma_s(E)$ and $\Sigma_p(E)$ begins by generating an initial guess for these quantities and then evaluating $\underline{G}^x$ from Eq. (4). New values of the Σ's are then determined from Eqs. (5) and (6), and the loop is repeated until the Σ's converge (convergence to 1.0×10^{-4} Ry was used). We did not encounter any numerical instabilities using this straightforward back-substitution method. However, more refined iterative methods may be needed for treating other systems. Once the self-energies are determined, the various densities of states and spectral functions may be calculated from Eqs. (4) and (7)–(10).

V. BAND STRUCTURES AND $n(E)$ AT STOICHIOMETRY

The energy bands and densities of states obtained from the LCAO Hamiltonian matrix are shown in Figs. 1–3 for $NbC_{1.0}$, $TaC_{1.0}$, and $HfC_{1.0}$. Table II gives further information relevant to these results; and Figs. 4–6 show planar sections of the Fermi surfaces of these compounds.

Although band structures and $n(E)$ for these stoichiometric carbides have been performed by other workers,[6,13,27–30] it is worthwhile to emphasize certain important features of our electronic-structure results and compare them with the previous works. We should emphasize that our calculations have been performed self-consistently and with relativistic corrections, both important effects. A detailed discussion of bonding in the carbides will be made in Sec. VI.

Referring to Figs. 1–3, we see that there is a great overall similarity between the energy bands and $n(E)$ for all three compounds. This can also be anticipated from Table I by noting the strong quantitative similarity of the LCAO parameters. The band-structure results for NbC and TaC having nine valence electrons per unit cell are nearly identical; while for HfC the Fermi level is shifted to a lower value corresponding to eight valence electrons per unit cell. In fact E_F falls near a minimum in $n(E)$ for HfC, and $n(E_F)$ has a value of approximately one-half of the other two carbides. Thus one can anticipate that the bonding in all three stoichiometric carbides considered is similar, with the major differences arising from changes in $n(E)$ and the Fermi surfaces resulting from the placement of E_F.

Examining Figs. 1–3 we find the lowest split-off occupied valence band to be primarily a carbon s band. Following is a gap and then a set of bonding bands consisting of carbon p states with some admixture of M d electrons. There is then a minimum in $n(E)$ followed by a set of fairly broad M d bands admixed with carbon p electrons. The higher conduction-band states consist of antibonding M d and C p states and M s and p bands. An important point to note is that the $n(E_F)$ values for NbC and TaC are rather low compared to the

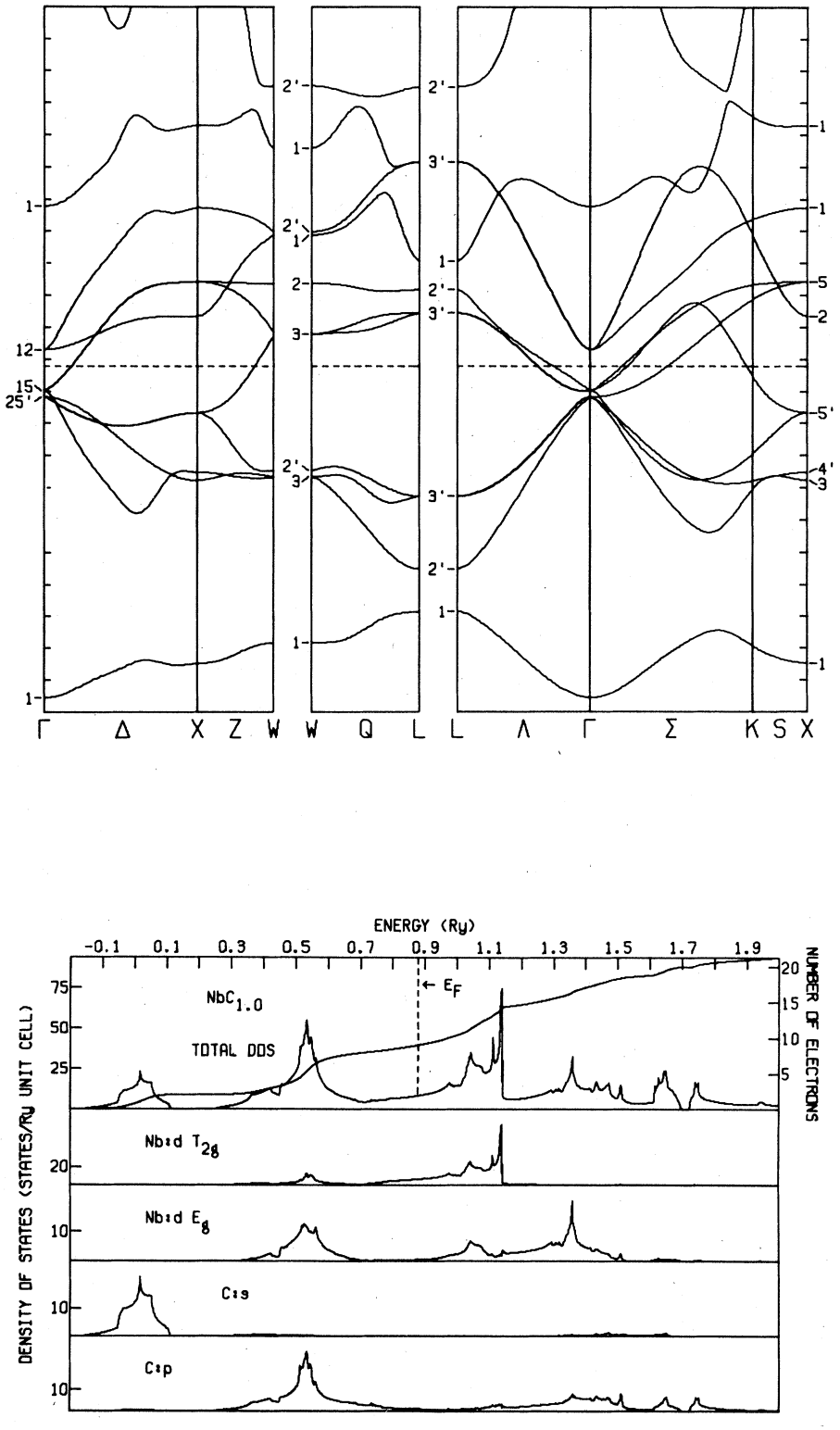

FIG. 1. Energy bands and densities of states for $NbC_{1.0}$.

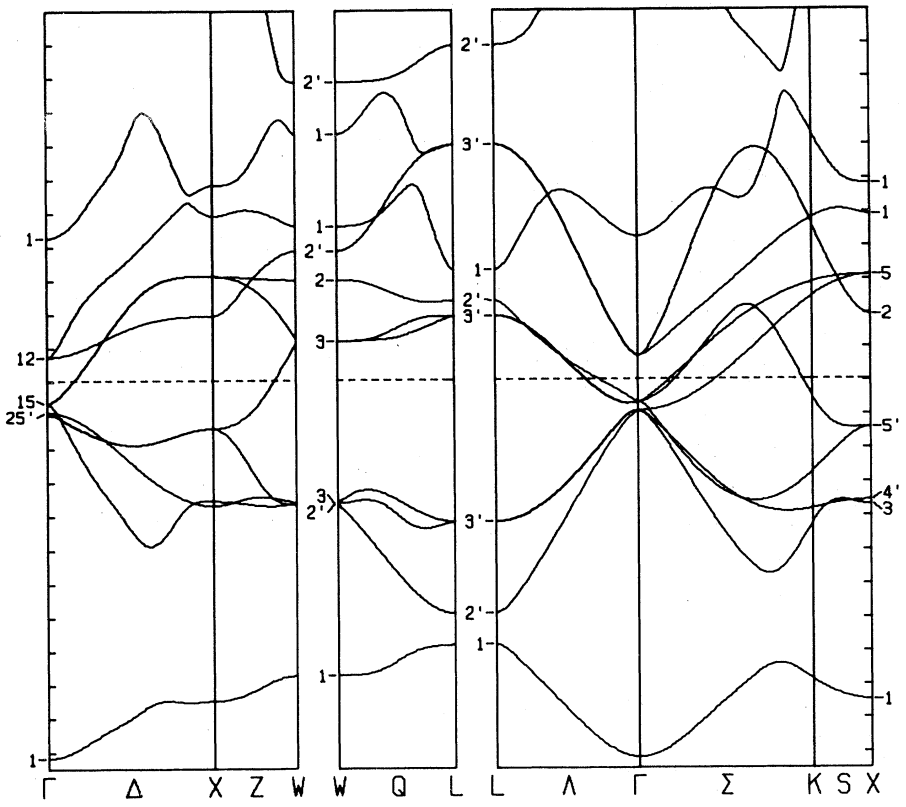

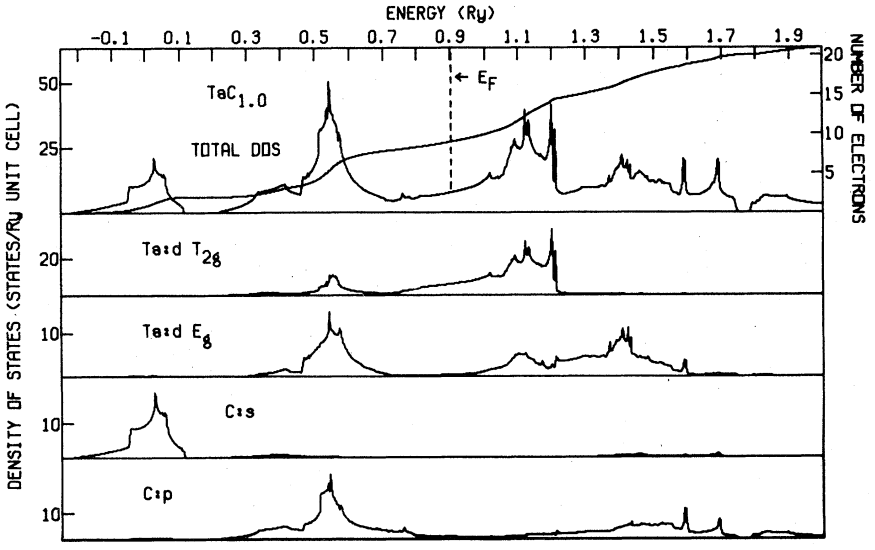

FIG. 2. Energy bands and densities of states for $TaC_{1.0}$.

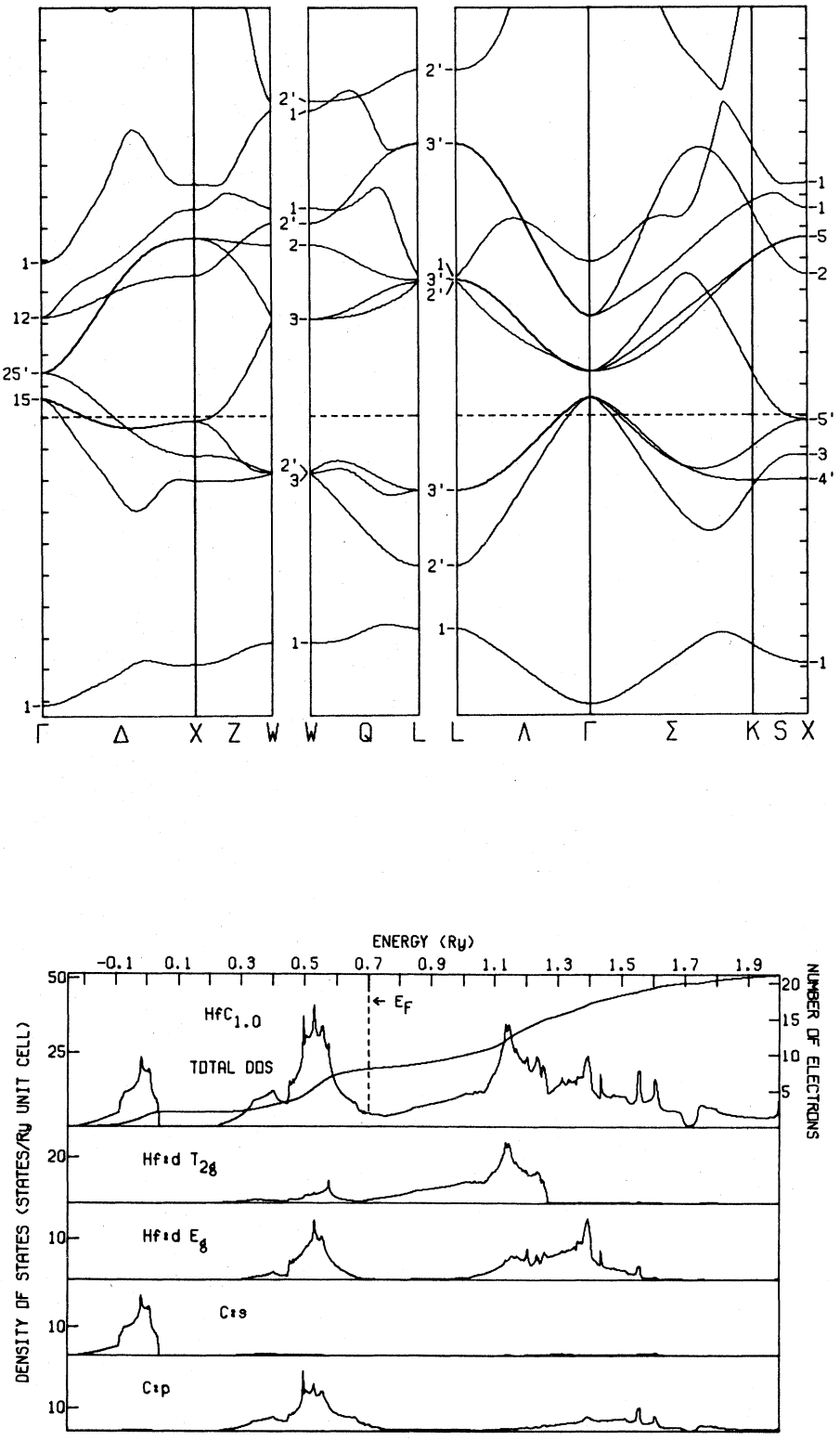

FIG. 3. Energy bands and densities of states for $HfC_{1.0}$.

TABLE II. Total densities of states at the Fermi level E_F, $n(E_F)$, for this and previous work for the stoichiometric carbides. Entries are in states per Ry per unit cell.

	$NbC_{1.0}$	$TaC_{1.0}$	$HfC_{1.0}$
Present work	8.33	7.67	4.55
Klein *et al.*[a]	9.52	8.66	1.84
Chadi and Cohen[b]	7.4		
Schwarz[c]	8.5		
Potorocha *et al.*[d]	6.8		
Ihara *et al.*[e]		8.84	2.18
Gupta and Freeman[f]	9.08	8.67	

[a] Reference 8.
[b] Reference 29.
[c] Reference 19.
[d] Reference 30.
[e] Reference 28.
[f] Reference 6.

parent d-band transition metals, being roughly one-half the values of Nb and Ta. And yet T_c is significantly higher for NbC and TaC than for Nb and Ta, respectively. We will come back to this point in Sec. VIII.

Comparing our band-structure results with those of other workers we find overall qualitative agreement. There are, however, rather large quantitative disparities as to the details of the band structures, especially with regard to the wave functions. This is not surprising since the majority of the previous calculations are not self-consistent, and, as we will discuss in the next section, there is a great deal of charge transfer in these compounds ($M \rightarrow C$). In situations where there is significant charge transfer and band hybridization SC effects are, in principle, important for a reliable band-structure picture. For instance, comparing our band orderings for NbC and TaC with those of Gupta and Freeman[6] we find several cases where C p and M d levels are interchanged. An example is the ordering of the Γ_{15}(C p-like) and Γ'_{25} (M d-like) levels just below E_F. Our SC results show that Γ'_{25} lies below Γ_{15}, while the Gupta and Freeman,[6] Ihara, *et al.*[28] and Chadi and Cohen[29] non-SC results are opposite. These kinds of band-ordering errors will propagate throughout the BZ owing to the necessity of satisfying compatibility relations. Therefore, although the Fermiology of some of the non-SC results are fortuitously similar to ours, the nature of the hybridized wave functions will, in general, be quite unreliable. In particular, the use of non-SC results for electron-phonon and phonon calculations, where electronic wave-function (or charge-density) effects are crucial, would be highly suspect. Schwarz's[13] SC band structure for NbC is very similar to ours with no band-ordering discrepancies. The differences that exist can be attributed to relativistic effects which we include and he does not. These shifts are ~10 mRy or less in most cases for NbC.

Despite the energy-band discrepancies just mentioned, the qualitative structure of the densities of states of all the MC calculations are similar. Table II gives values of $n(E_F)$ for the different calculations in the literature. We also show for completeness the values we had previously obtained[8] using the QUAD method[31] for an 89-$\vec{k}$-point mesh (NbC and TaC), and a 20-$\vec{k}$-point mesh (HfC) in the IBZ. The large difference in $n(E_F)$ for HfC between the LCAO and APW-QUAD $n(E_F)$ results is probably due to poor $\vec{k}$-point convergence of the latter calculation. However, since E_F falls near a minimum in $n(E)$, it is possible that in this case the $n(E_F)$ value for the LCAO calculation is sensitive to the fitting errors of the LCAO Hamiltonian in this region. For NbC and TaC the differences in $n(E_F)$ between our LCAO and APW-QUAD results are ~15%. Fortunately, none of the results or conclusions in this paper is very sensitive to this kind of error.

The Fermi surfaces of the three carbides are shown in Figs. 4–6 for several planes in the BZ. The large band-5 surface of NbC and TaC correspond to a three-dimensional jungle-gym centered around Γ with rather flat parallel arm surfaces over large regions of $\vec{k}$ space. This "nesting" feature has been shown to lead to anomalous peaks in the susceptibility function $\chi_0(\vec{q})$ for values of $\vec{q}$ which can be related to the geometry of this Fermi surface.[6-8] Furthermore, since $\chi_0(\vec{q})$ is a critical element determining the phonon-dispersion curves, these peaks can be related to the occurrence of the phonon anomalies, or dips in the dispersion curves in these materials. As can be seen from Fig. 6, no such jungle-gym surface exists for HfC, and the $\chi_0(\vec{q})$ anomaly is not present, nor are there phonon anomalies. In Sec. VII we discuss further the relationship between the phonon anomalies and the charge density and Fermi surfaces of the carbides. In particular, we use the CPA results of Sec. VI regarding the changes in

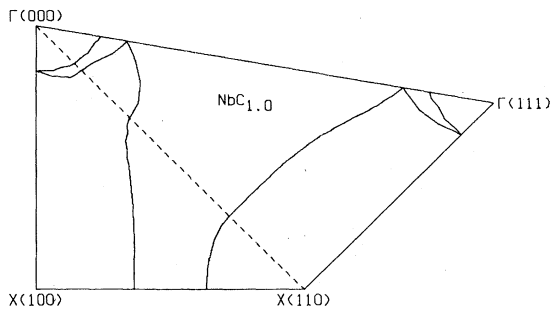

FIG. 4. Fermi-surface cross sections for $NbC_{1.0}$.

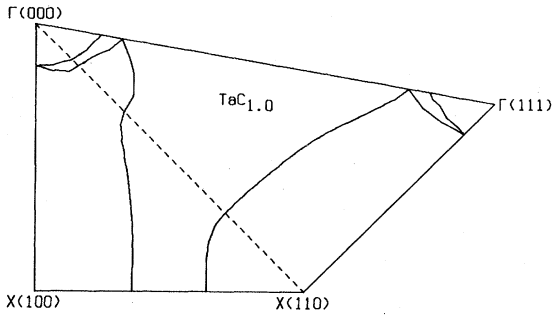

FIG. 5. Fermi-surface cross sections for $TaC_{1.0}$.

the Fermi surfaces upon the introduction of carbon vacancies to explain the vanishing of the phonon anomalies in this case. Finally we should mention that attempts to measure the stoichiometric Fermi surfaces have, up to now, failed owing to the lack of availability of crystals with less than ~1% vacancies. The de Haas-van Alphen measurements tried so far have not been able to resolve the Fermi surfaces because of this.[32]

VI. CPA RESULTS

Densities of states and self-energies

In Figs. 7–9 we show the CPA-derived densities of states for NbC_x, TaC_x, and HfC_x for the cases $x = 1.0$, 0.9, 0.8, and 0.7; and Table III gives some additional information. It is very interesting to note the overall similarity among all these curves, with the major differences being the location of $E_F(x)$. The latter has been determined by integrating $n(E)$ up to 9.0, 8.6, 8.2, and 7.6 electrons for NbC_x and TaC_x, and 8.0, 7.6, 7.2, and 6.8 electrons for HfC_x, respectively. By comparing the results for different values of x, it is seen that there is no significantly new structure introduced into the $n(E)$ curves by the carbon vacancies other than an overall broadening of the sharp features. At first glance one would tend to say that a rigid-band-type picture for treating the vacancies appears to hold, but noticing that $E_F(x)$ goes up with decreasing x (more vacancies), one can anticipate our discussion below which emphasizes some important subtleties of interpre-

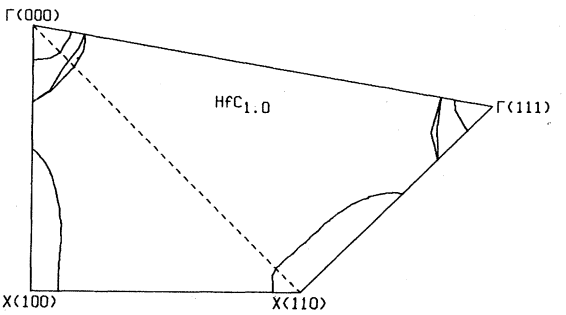

FIG. 6. Fermi-surface cross sections for $HfC_{1.0}$.

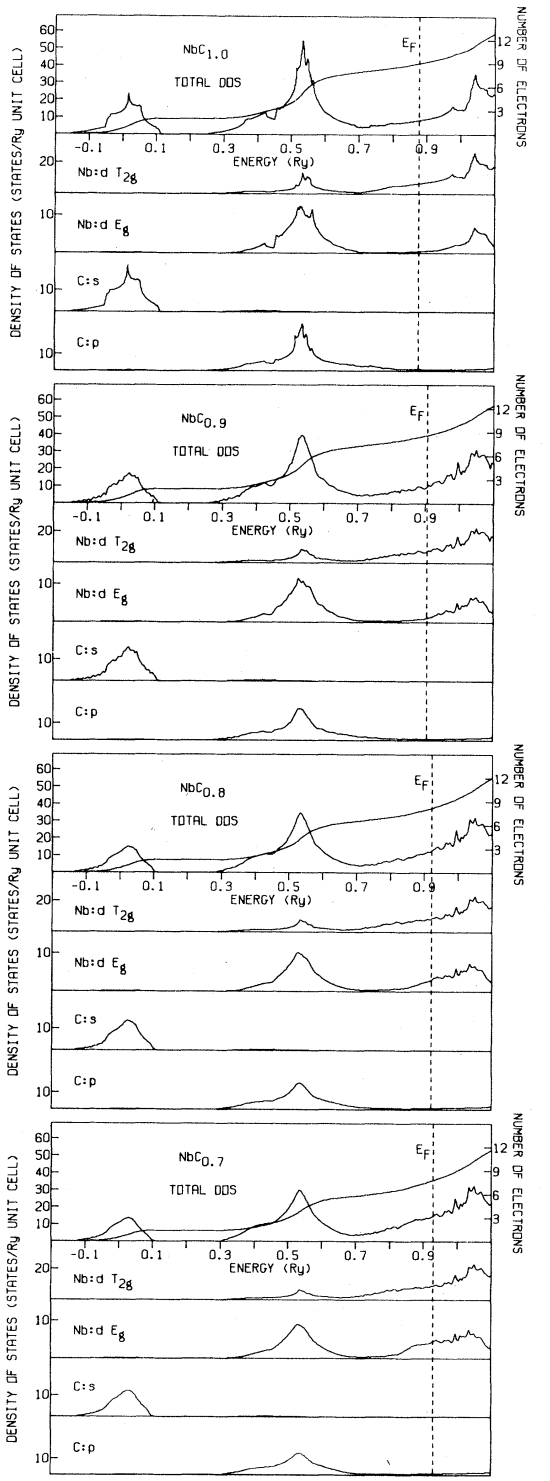

FIG. 7. Densities of states for NbC_x.

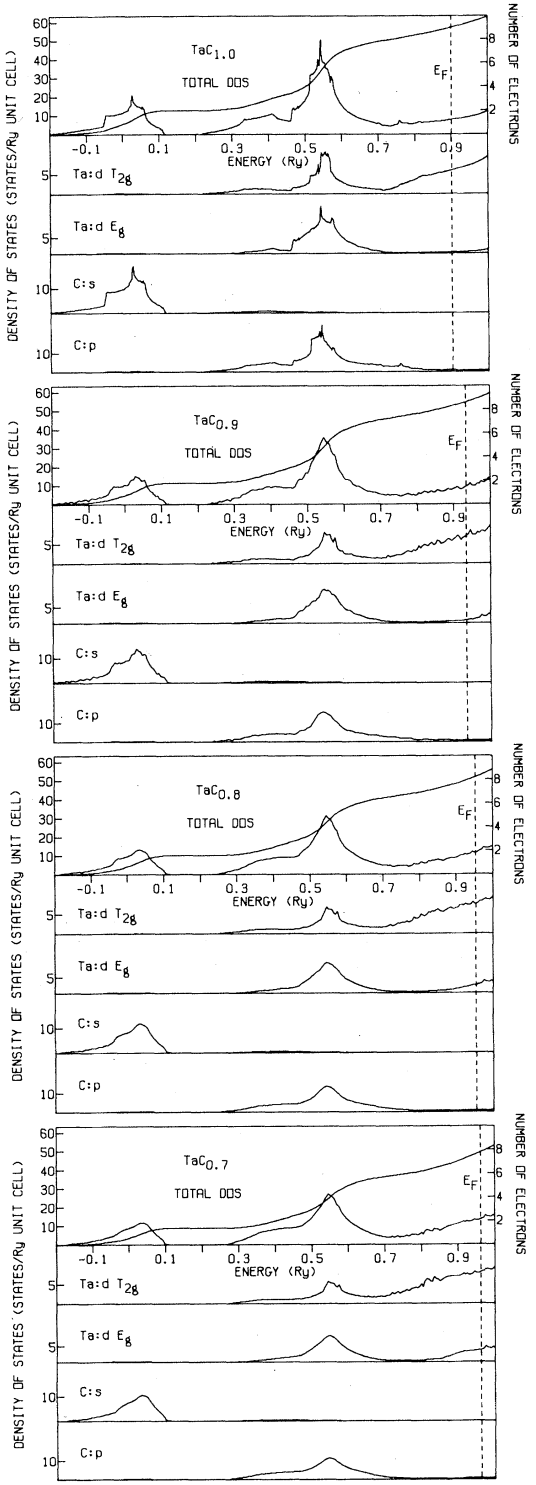

FIG. 8. Densities of states for TaC_x.

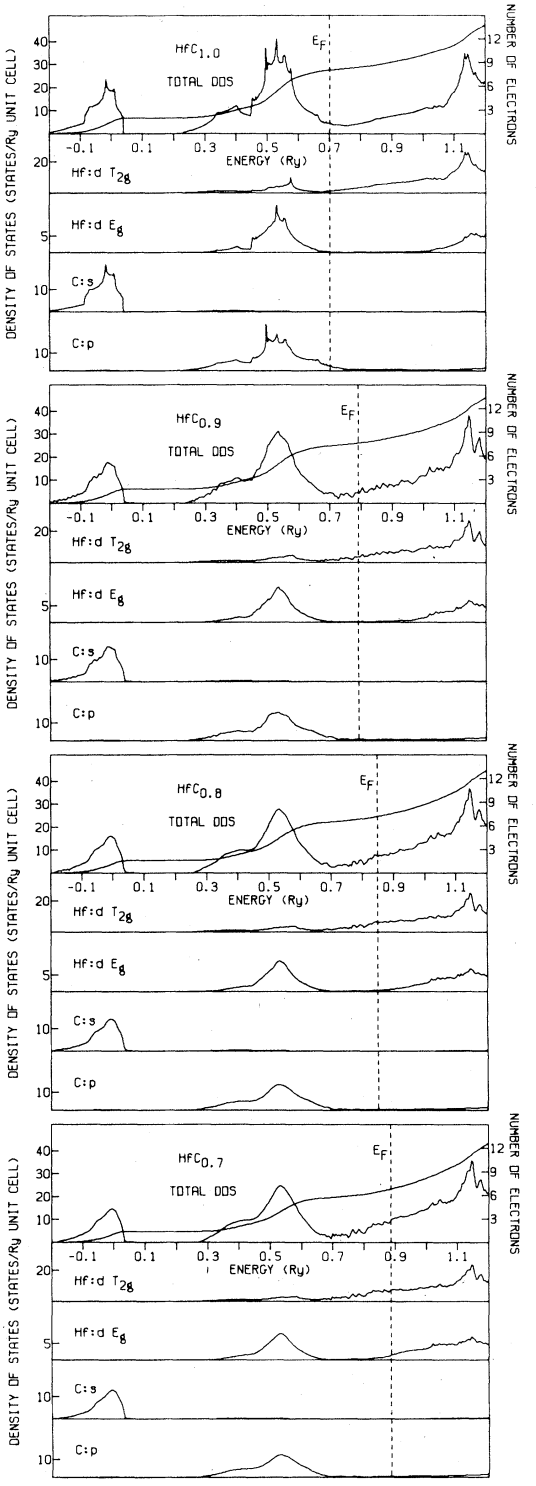

FIG. 9. Densities of states for HfC_x.

tation regarding the use of a rigid-band picture. Values of E_F, $n(E_F)$, and $n_l^i(E_F)$ are given in Table III for the four values of x.

Figures 10 and 11 show the s and p complex self-energies for $NbC_{0.8}$. It is interesting to note that the imaginary parts of the self-energies which, in a broad sense, give a measure of the disorder-induced damping of the electron quasi-

TABLE III. Fermi energies E_F; total (n) and site angular momentum decomposed (n_l^i) densities of states at E_F; energy-integrated densities of states ($N_l^i \equiv \int_{-\infty}^{E_F} n_l^i(E)dE$). E_F are in Ry, n are in states per Ry unit cell, and N_l^i are electrons.

	E_F	n	n_s^M	n_p^M	$n_d^M{}_{E_g}$	$n_d^M{}_{T_{2g}}$	n_s^C	n_p^C	N_s^M	N_p^M	$N_d^M{}_{E_g}$	$N_d^M{}_{T_{2g}}$	N_{tot}^M	N_s^C	N_p^C	N_{tot}^C
$NbC_{1.0}$	0.877	8.331	0.137	0.230	0.451	6.498	0.006	1.009	0.457	0.256	1.517	1.735	3.965	1.826	3.209	5.035
$NbC_{0.9}$	0.905	9.735	0.142	0.236	1.120	7.372	0.019	0.846	0.463	0.235	1.501	1.913	4.112	1.634	2.854	4.488
$NbC_{0.8}$	0.922	12.885	0.208	0.282	2.962	8.514	0.040	0.879	0.439	0.216	1.501	2.094	4.250	1.447	2.503	3.950
$NbC_{0.7}$	0.930	15.206	0.252	0.306	4.724	9.000	0.048	0.876	0.416	0.198	1.552	2.212	4.377	1.266	2.158	3.424
$TaC_{1.0}$	0.901	7.670	0.179	0.228	0.374	5.975	0.009	0.906	0.543	0.256	1.477	1.724	4.000	1.837	3.165	5.002
$TaC_{0.9}$	0.933	9.272	0.214	0.254	0.934	7.058	0.018	0.792	0.554	0.237	1.457	1.899	4.147	1.636	2.817	4.453
$TaC_{0.8}$	0.953	11.442	0.278	0.282	2.498	7.584	0.042	0.760	0.529	0.218	1.440	2.094	4.281	1.450	2.469	3.919
$TaC_{0.7}$	0.963	13.502	0.356	0.308	3.840	8.176	0.051	0.772	0.505	0.201	1.478	2.219	4.404	1.268	2.128	3.396
$HfC_{1.0}$	0.701	4.547	0.028	0.230	0.169	1.287	0.008	2.825	0.489	0.267	1.328	0.828	2.912	1.812	3.275	5.087
$HfC_{0.9}$	0.791	4.475	0.047	0.118	3.465	0.151	0.004	0.689	0.497	0.251	1.275	0.968	2.991	1.619	2.990	4.609
$HfC_{0.8}$	0.848	7.382	0.083	0.183	6.166	0.407	0.014	0.528	0.469	0.234	1.177	1.242	3.122	1.431	2.647	4.079
$HfC_{0.7}$	0.886	9.528	0.211	0.337	7.084	1.405	0.055	0.436	0.442	0.218	1.097	1.496	3.253	1.253	2.294	3.547

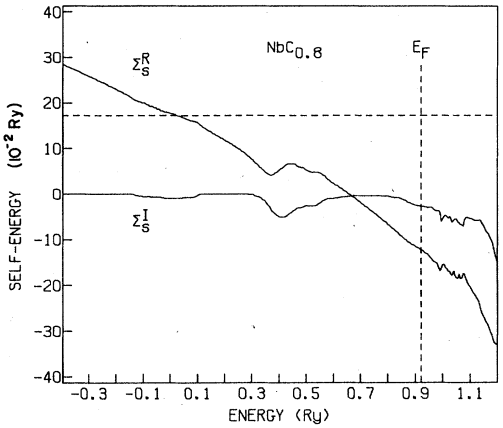

FIG. 10. Complex s self-energy for $NbC_{0.8}$. Σ_s^R is the real part, and Σ_s^I is the imaginary part. The horizontal dashed line is $E_{s_2,s_2}(000)$.

particles, show a large variation near E_F. One would therefore expect that the disorder scattering would have a large effect on the Fermi surfaces of the vacancy materials in a non-rigid-band manner. This has important consequences regarding the phonon and superconducting properties of these materials, as we will discuss below.

Charge transfer

There has been some controversy in the literature regarding the nature of the charge transfer and bonding in the carbides. While all of the SC muffin-tin band-structure calculations, including ours, show a transfer of electrons from the M sphere to the C sphere during self-consistency, our LCAO fit gives further support to a charge transfer from $M \rightarrow$ C without the muffin-tin constraint. Table III gives the populations of the oc-

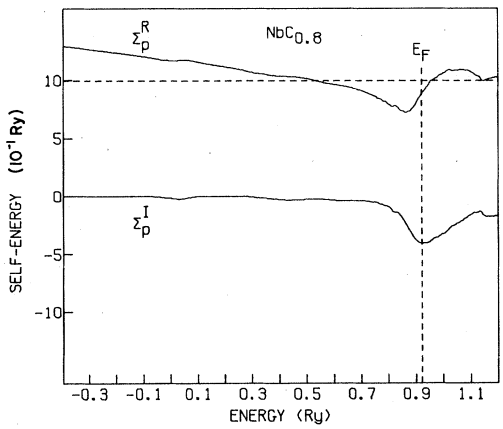

FIG. 11. Complex p self-energy for $NbC_{0.8}$. Σ_p^R is the real part, and Σ_p^I is the imaginary part. The horizontal dashed line is $E_{x_2,x_2}(000)$.

cupied orbitals for the carbides obtained by integrating the $n_l^j(E)$ from the bottom of the lowest-occupied valence band up to E_F.

From Table III we see that at stoichiometry there is an excess ~1.0 electrons associated with the C orbitals compared to the free-atom occupations. Keeping in mind that the SC-APW charge shift is ~0.5 electrons from the $M \rightarrow$ C muffin-tin spheres, we see that both the LCAO and APW pictures of charge transfer are qualitatively the same (the LCAO charge shift refers to the entire unit cell, while the APW picture leaves the interstitial charge density uncharacterized). There seems to be no doubt that the charge transfer is $M \rightarrow$ C, in agreement with the electron-spectroscopy-for-chemical-analysis (ESCA) measurement analysis of Ramquist.[33] This latter analysis shows an excess of ~0.5 electrons associated with the C site. However a detailed quantitative relationship between the ESCA measurements and our LCAO or APW charge analysis does not seem to be possible because the quantitative definitions of charge transfer are not precisely related.[34]

This charge transfer has important consequences regarding the motion of the Fermi level when carbon vacancies are introduced ($x < 1.0$). Because of the charge transfer, when a carbon atom is removed from the system ~5.0 states are emptied although only 4.0 electrons are removed, and ~1.0 electrons are transferred back to the M. In the rigid-band sense, the extra M electron cannot fill the emptied C states, but must instead occupy empty d states above the original Fermi level. The new Fermi level is therefore higher. This simplified interpretation has been verified by the results of our CPA calculations displayed in Table III. Notice that as x decreases, the number of occupied M d electrons increases roughly in proportion to what would be predicted from the above arguments.

We emphasize that it is unreliable to apply rigid-band arguments blindly to the case of binary compounds with substitutional impurities (including vacancies). Our carbide results show how important it is to know the bonding characteristics of the host compound in predicting Fermi-level motion with impurities. For the case of vacancies in a binary compound three cases can exist: (1) The AB stoichiometric compound has no charge transfer, so that B vacancies leave the Fermi level unchanged; (2) charge transfer is from $B \rightarrow A$ so that with B vacancies E_F moves down; (3) charge transfer is from $A \rightarrow B$ so that E_F moves to higher energy as the number of B vacancies goes up. The latter is the case of the refractory monocarbides. Case (2) corresponds to the situation for PdH_x which we have studied previously[25] using a similar LCAO–CPA approach. We found that for $PdH_{1.0}$ only 0.2 H electrons were in occupied states and the rigid-band prediction of E_F moving down with x was also verified by the CPA calculations. However in the case of PdH_x the predicted charge-transfer direction and magnitude determined from the APW method was very sensitive to the choices of Pd and H muffin-tin radii although the band-structure results were not. If the H-sphere radius was chosen too large, the charge transfer was seemingly in the opposite direction (Pd→ H). We believe the LCAO representation, not being shackled by the artificial muffin tins, gives a more reliable picture of charge-transfer effects.

Bonding

Most theories have emphasized the M-C covalent bonding as being important for understanding the physical properties of the carbides.[1] From general chemical and wave-function-symmetry considerations one can show that the M d E_g orbitals can hybridize with the carbon sp orbitals forming σ bonds, and the M d T_{2g} orbitals can form π bonds with the carbon p electrons. Evidence for the strong covalent bonds in the carbides comes from our results in Table III where it is evident that the $M \rightarrow$ C charge transfer has been primarily from the M d T_{2g} states to the carbon p states. Note that for $x < 1.0$ this d T_{2g} charge is transferred back to the M atom. This point is further emphasized by calculating the ratio $N^M_{d\text{-}T_{2g}}/N^M_{d\text{-}E_g}$ which has the value 1.1, 1.1, and 0.6 for $NbC_{1.0}$, $TaC_{1.0}$, and $HfC_{1.0}$, respectively. For an isotropic system this ratio would be 3 : 2, but the d T_{2g} charge depletion has considerably reduced this number, especially for $HfC_{1.0}$. (Note that any nonspherical environment will lead to deviations from the 3 : 2 ratio, even in the simple bcc transition metals Nb and Ta. These deviations are usually much smaller than that of $HfC_{1.0}$.) From the $HfC_{1.0}$ results it is clear that the covalent-bonding states are particularly strong below the minimum in the density of states where E_F for $HfC_{1.0}$ falls (see Fig. 3). Above this minimum, the extra electron in $NbC_{1.0}$ and $TaC_{1.0}$ goes primarily into filling d T_{2g} states and there is no further charge transfer beyond that of $HfC_{1.0}$.

The overall picture is that in approaching stoichiometry, the charge transfer from the M d T_{2g} states strengthens the M-C bonds but weakens the M-M bonds. As carbon is removed, charge is transferred back to the M d T_{2g} states and the M-M bonds are strengthened. Furthermore, the charge transfer and covalent bonding are essentially complete in $HfC_{1.0}$, with the extra electron in $NbC_{1.0}$ and $TaC_{1.0}$ filling metallic

$d\,T_{2g}$ states leading to the enhanced metallic behavior of the latter two compounds.

Finally one can use these arguments to understand why it is so difficult to make stoichiometric carbides having x values close to unity. The approach to stoichiometry can be characterized by the diffusion of carbon from the crystal surface into the bulk, filling holes in the fcc lattice. The diffusion proceeds by the process of a moving carbon atom colliding with another carbon atom on an occupied site, knocking it out of its parent site further into the bulk. This continues until all carbon sites are filled and additional carbon atoms are inhibited from crossing the surface. Because the carbon atoms are so strongly bound in the carbide lattice, it is energetically very costly to bump a carbon atom off its occupied site, and therefore it is difficult for the diffusion process to lead to stoichiometry. These ideas are consistent with the discussion of carbide preparation given in Toth's book.[1]

Fermi surfaces

As noted earlier, one can correctly predict the motion of the Fermi level for the substoichiometric carbides using a rigid-band model when proper account is taken of charge transfer. We also pointed out in Sec. VI that the existence of substantial damping caused by disorder scattering, or a relatively large value of the imaginary part of the self-energy near $E_F(x)$, would lead to nonrigid-band behavior of the Fermi surfaces. We illustrate this in Fig. 12, where we show examples of the band-5 substoichiometric Fermi surfaces of $NbC_{0.9}$ and $NbC_{0.8}$ calculated either from the rigid-band model or from the CPA Bloch spectral function,

$$A(\vec{k}, E_F) \equiv -\frac{1}{\pi}\,\mathrm{Im}\sum_{i=1}^{13} G^{x}_{i,i}(\vec{k}, E_F)\,.$$

Comparing Fig. 12 with Fig. 4, we see that the main effect of the rigid-band model for $x < 1.0$ is to increase the dimensions of the jungle-gym arms; while the CPA results additionally introduce considerable smearing of the nesting features. The smearing increases with decreasing x, and at $x = 0.9$, the half-width is $\sim 0.1(\pi/a)$, a value as large as the phase-space width of the phonon anomalies in these materials. At $x = 0.8$, the jungle-gym surface is nearly completely washed out. As we discuss below, this Fermi-surface smearing is important for understanding the phonon, superconducting, and other properties. The smearing of TaC_x (not shown) is very similar to NbC_x.

Finally, we urge that experimental Compton scattering and positron annihilation measurements

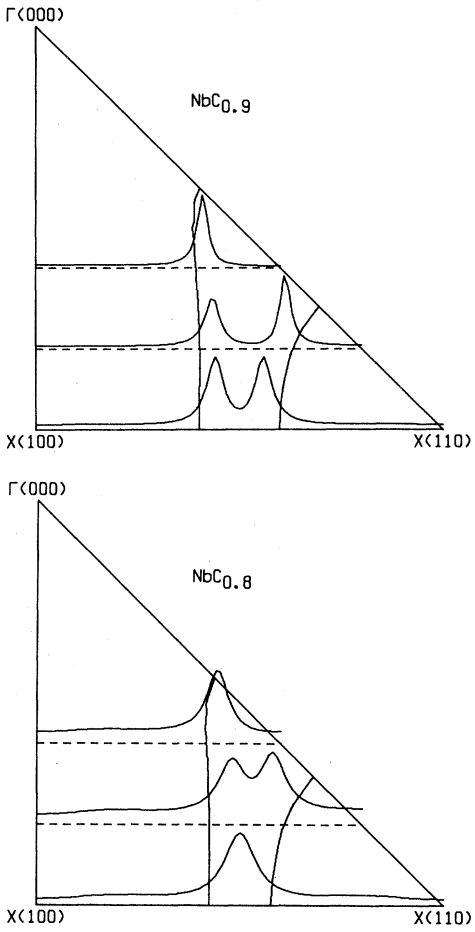

FIG. 12. Fermi-surface cross sections for $NbC_{0.9}$ and $NbC_{0.8}$ for band 5. The solid curves (nearly vertical) are the jungle-gym surface obtained using the rigid-band model. The peaked curves are the Bloch spectral functions [Eq. (7)] plotted for the $\vec{k}$ lines shown by the dashed lines. The amplitude of the Bloch spectral functions are the vertical heights (arbitrary units).

be performed on the carbides. As is well known, carbon vacancies do not affect the viability of such measurements as they do for the de Haas-van Alphen experiments. The former two experiments would allow a very useful comparison with our CPA results, as the x dependence of the Fermi-surface smearing that we calculate should be observable.

VII. PHONON ANOMALIES

Smith and Gläser[3] have measured phonon-dispersion curves for several MC compounds. They found that at certain wave vectors there were phonon anomalies for the superconductors NbC and TaC. These anomalies were absent in nonsuperconducting HfC and ZrC. It has also been observed that the phonon anomalies tend to disap-

pear as the number of carbon vacancies is increased.[3]

Weber *et al.*[4,5] have performed accurate calculations of the phonon-dispersion curves of the carbides using the "double-shell model." Weber found[5] that the model parameters needed to obtain a good fit to experiment, including an explanation of the phonon anomalies, showed that for $NbC_{1.0}$ and $TaC_{1.0}$ there was a resonance-like increase of the electronic polarizability of the d electrons having T_{2g} symmetry. Subsequently, Gupta and Freeman,[6] and Klein *et al.*[7,8] showed that the phonon anomalies might be related to peaks in the electronic susceptibility $\chi_0(\vec{q})$, caused by scattering of electrons across the fifth-band Fermi surfaces shown in Figs. 4 and 5. They argued[6-8] that there is a large overscreening of the bare interactions, especially at selected wave vectors corresponding to the dimensions of the nested Fermi surface. Although not explicitly demonstrated, it was assumed that the $\chi_0(\vec{q})$ anomalies were related to the T_{2g} resonances in Weber's model.

The present CPA calculations offer some further insights into this problem. From our previous discussion we note that at stoichiometry there has been a charge transfer from the metal d T_{2g} states to the carbon p states. We argue that the reduced T_{2g} charge density leads to weakened M–M bonds, which makes them susceptible to strong charge fluctuations. For NbC and TaC this fact coupled with the nested Fermi surface, which enhances the electron-phonon scattering in the T_{2g} bonds, is likely to drive the phonon anomalies. In HfC, although the T_{2g} bonds are also relatively weak, there are no nested Fermi-surface features to drive an instability.

As carbon atoms are removed, charge is transferred back to the T_{2g} bonds and they are strengthened. This together with the disorder smearing of the nested Fermi surface leads to an increased stability of the T_{2g} bonds and the vanishing of the phonon anomalies in NbC_x and TaC_x ($x < 1.0$).

In order to verify the qualitative conjectures just put forth, explicit phonon-spectra calculations, including the effects of vacancy disorder, would have to be made. Extensions of the LCAO-phonon approach of Varma and Weber,[35] successful for stoichiometric transition metals, appears to be the most promising for examining these questions. Splettstösser[36] has already made some progress in this direction. He has used a force-constant model to study the effects of C vacancies on the phonon spectra of NbC_x using a simplification of Weber's shell-model approach. He argues that the disappearance of the phonon anomalies in TaC_x and NbC_x when $x \sim 0.8$ is related to a stabilization of the second-neighbor Nb-Nb interactions upon removal of carbon atoms. It would be interesting to develop relationships between our theoretical results and Splettstösser's model.

VIII. SUPERCONDUCTIVITY

Experiments show that NbC_x and TaC_x are superconductors with $T_c \sim 11$ K for the stoichiometric materials ($x = 1.0$). It is found that $T_c(x)$ falls monotonically with increasing numbers of carbon vacancies with $T_c(0.8) \sim 1.0$ K. It has been further observed that HfC_x is not superconducting for any value of x. In this section we will discuss the superconducting properties of the carbides making use of both our APW and LCAO–CPA results. The discussion for the substoichiometric materials will be qualitative and somewhat conjectural due to the lack of a good quantitative theory of superconductivity for vacancy systems such as these.

Superconducting transition temperatures are usually calculated from McMillan-type formulas of the form[37]

$$T_c = (\bar{\omega}/1.2)\exp[-1.04(1+\lambda)/\lambda - \mu^*(1.0+0.62\lambda)], \tag{11}$$

with

$$\lambda = \sum_j \lambda_j = \sum_j \frac{n(E_F)I_j^2}{M_j\langle\omega^2\rangle_j}. \tag{12}$$

Here I_j^2 is a Fermi-surface-averaged electron-phonon matrix element, M_j is the mass of atom j in the unit cell, μ^* is the Coulomb pseudopotential, and $\langle\omega^2\rangle_j$ and $\bar{\omega}$ are phonon-spectra moments defined in Ref. 8. Equations (11) and (12) are generalizations to compounds[2,38] of the original approach taken by McMillan.

Klein *et al.*[2,8] have previously discussed superconductivity for the stoichiometric carbides by using the APW results together with the theory of Gaspari and Gyorffy (GG)[39] to calculate the nI_j^2 and the phonon moments calculated from the measured phonon-dispersion curves.[3] For reasonable values of $\mu^* \sim 0.1$ they obtained good agreement with experiment for $T_c(x = 1.0)$.[2,38] For $x < 1.0$ one is faced with calculating the new "electronic factors," nI_j^2, and the new phononic moments $\langle\omega^2\rangle_j$ and $\bar{\omega}$ for the substoichiometric systems.

As we mentioned in the preceding section, the phonon spectra of NbC_x and TaC_x have anomalous dips at stoichiometry which vanish with increasing numbers of carbon vacancies.[3] This translates into an increase in $\langle\omega^2\rangle_j$ and $\bar{\omega}$ as x decreases, an effect which tends to lower λ but increases the prefactor in Eq. (11). Since λ enters Eq. (11) exponentially, the overall effect of phonon stiffen-

ing is to depress T_c as x decreases. However the electronic factors nI_j^2, of course, also have an x dependence which has to be considered.

One can attempt to estimate the x dependence of nI_j^2 by using rigid-band types of arguments, i.e., using the LCAO–CPA values of $E_F(x)$ to evaluate nI_j^2 from the APW results with the GG theory. We have done this previously for the carbides,[40] and we found that nI_j^2 actually increases as x decreases, largely cancelling out the observed phonon stiffening in the denominator of Eq. (12) and leading to T_c decreasing with x only when excess phonon stiffening is used (approximately twice the observed amount of increase in $\bar{\omega}$ and $\langle\omega^2\rangle_j$). We believe that the rigid-band approach for estimating T_c fails because of the neglect of lifetime or Fermi-surface smearing effects in these systems in calculating nI_j^2. We will now attempt to give some justification to this assertion.

Although the values of $n(E_F)$ for $NbC_{1.0}$ and $TaC_{1.0}$ are approximately one-half the values of the parent transition metals, their rigid-muffin-tin values of I_M^2 are significantly larger. We believe that the large values of I_j^2 are related to enhanced electron-phonon scattering across the fifth-band jungle-gym Fermi surfaces shown in Figs. 4 and 5. These Fermi-surface pieces have already been shown to lead to enhancements in the susceptibility function entering into phonon theory,[6-8] and it appears reasonable to assume that they are also responsible for enhancing I_j^2. Indeed the major contribution to the electronic states at E_F comes from band 5 (by far the biggest piece of Fermi surface). The resultant effect on λ would presumably be even greater were it not for the so-called "constant α^2" approximation[38] that has been used in conjunction with the GG theory which tends to wash out any resonant behavior. The reason that we emphasize this point is that, from Fig. 12, we see that there is a great deal of disorder smearing of these Fermi surfaces for $x < 1.0$, and resonant-type electron-phonon scattering across the jungle-gym arms will no longer be present. Even if one defines a sharp Fermi surface for the disordered material to match the peaks in the Bloch spectral function (see Fig. 12), the nesting features are still quickly lost in going away from stoichiometry. These Fermi-surface effects are not given correctly in a rigid-band description where we find that I_j^2 remains roughly a constant with changing x. The rigid-band result is that nI_j^2 increases because $n(E_F)$ increases with decreasing x. Proper account of Fermi-surface smearing effects would lead, we believe, to a considerable reduction in I_j^2 as x decreases and would not require invoking the unphysically large amount of phonon stiffening to explain $T_c(x)$.[40] Unfortunately, theories of nI_j^2 which take into account lifetime or Fermi-surface smearing effects are not available to add quantitative muscle to these arguments. We intend to pursue this question further in subsequent work.

Additional support for our assertion of the importance of the jungle-gym Fermi-surface smearing in the carbides comes from our previous rigid-band and CPA work on PdH_x.[25] In those compounds the rigid-band calculated values of T_c were in good agreement with the experimental values as a function of x. We would argue that this is because there are no Fermi-surface nesting features present for the stoichiometric case, and that disorder scattering effects are much less important. To check this point we have calculated the Fermi surface of $PdH_{1.0}$, and, indeed, for this compound, nesting features are absent. In fact the $PdH_{1.0}$ Fermi surface appears very similar to copper or silver, being nearly spherical with necks at the L point. Note also that there have been no phonon anomalies observed for $PdH_{1.0}$ of the type present in the carbides.

Finally we comment on some previous work done to describe superconductivity in the substoichiometric carbides. Ries and Winter[41] and Schwarz and Rösch[42] have done cluster calculations for NbC with and without a carbon vacancy. The former authors[41] considered clusters of up to 203 atoms, 14 shells in all, surrounding a central carbon atom or vacancy. The latter authors[42] considered much smaller clusters of the form $CNb_6C_{12}Nb_8$ or [vacancy] $Nb_6C_{12}Nb_8$. In both works the goal was to study the effects of carbon vacancies on the electron-phonon interaction and T_c.

Although Ries and Winter[41] appear to have obtained good convergence with their stoichiometric cluster, the central-site-vacancy case corresponds to $x \sim 0.99$, a very dilute vacancy situation. They find that E_F is nearly unchanged for the single-vacancy case and that $\Delta n/\Delta x > 0$ so that the total density of states at E_F goes down with the single vacancy. They extrapolate these results for $x \sim 0.99$ to study superconductivity in the range $0.8 \leq x \leq 1.0$. We believe that such an extrapolation from the very dilute vacancy case is very questionable especially since our CPA results (and those of Klima[10]), and the physical arguments we have made regarding the charge transfer show that E_F moves to higher energy as x decreases substantially, and also $n(E_F)$ increases.

Schwarz and Rösch[42] attribute the scattering of metal d electrons into the empty nonmetal p states as being responsible for the phonon softening and the dependence of T_c on carbon vacancies. They find that as x decreases the formerly empty carbon

p states just above E_F become filled, causing T_c to decrease. Although our CPA results are not necessarily in contradiction with the cluster calculations of Schwarz and Rösch,[42] the small cluster size that they have considered casts doubt on the conclusions they have reached.

We would recommend that people doing cluster calculations extend their calculations to converged configurations with 10% or more carbon vacancies in order to draw convincing conclusions regarding the effects on physical properties. In addition, both sets of cluster calculations have neglected the lifetime effects that we have just discussed. These effects should be important in interpreting the cluster results for exactly the same reasons.

IX. COMPARISON WITH PHOTOELECTRON SPECTRA

There have been several recent photoelectron-spectra measurements for the carbides that we have studied.[28,43] In order to compare with these measurements we have taken our total densities of states $n(E,x)$ and broadened them with a Lorentzian with the full width half maximum (FWHM) γ. In this approximation we have neglected matrix-element effects, sacrificing some numerical accuracy for the sake of a great computational simplification. The removal of this approximation would alter the energy dependences of the absolute intensities but probably not the peak locations. Figures 13–15 show our calculated spectra for $\gamma = 1.0$ eV and the experimental spectra. Table IV lists the theoretical and experimental locations of the three most prominent peaks in the spectra. Since we have neglected matrix-element effects we have not optimized the fits (by varying γ) to try and reproduce the experimental peak widths. We note that the peak locations do not shift by increasing γ, although doing so broadens the spectra in an obvious manner (some washing out of sharp features). We also note that the downward shift in peak locations with increasing carbon vacancies are due almost entirely to the motion of $E_F(x)$.

The overall agreement with the experimental spectra is quite good with the biggest peak-location discrepancy corresponding to HfC if the experimental samples are very close to stoichiometry. Ihara *et al.*[28] do not quote the x value for their samples, but they do remark that "the ratios of combined carbon to metal atoms of the powders were above 0.98." These powders were subsequently hot pressed to form the samples, so that the ultimate stoichiometry is apparently

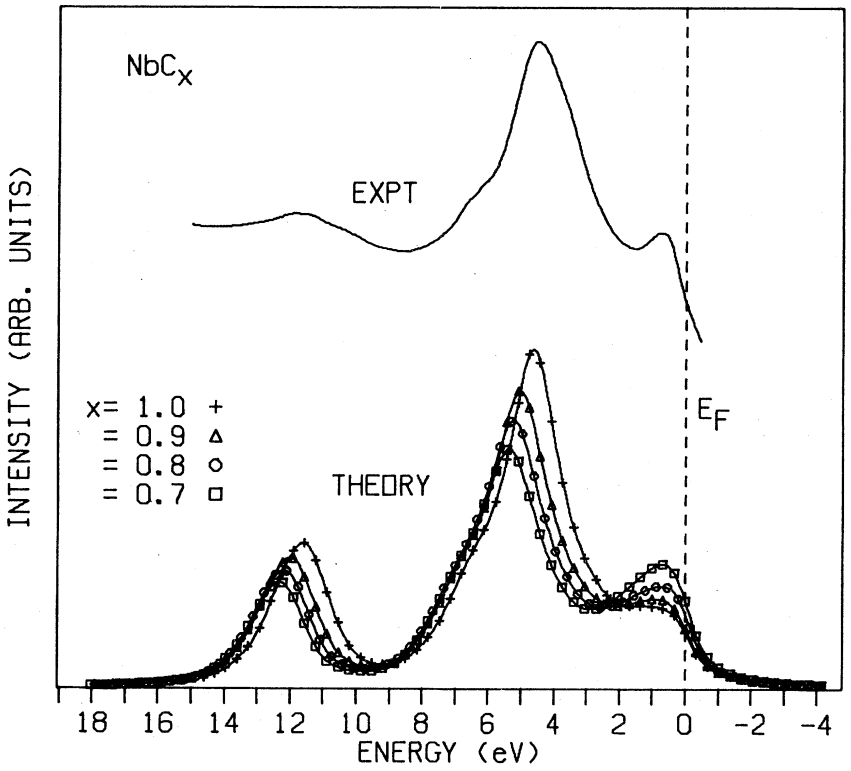

FIG. 13. Experimental photoelectron spectrum of Ref. 43 (top curve), and Lorentzian-broadened total densities of states ($\gamma = 1.0$ eV FWHM) for NbC$_x$.

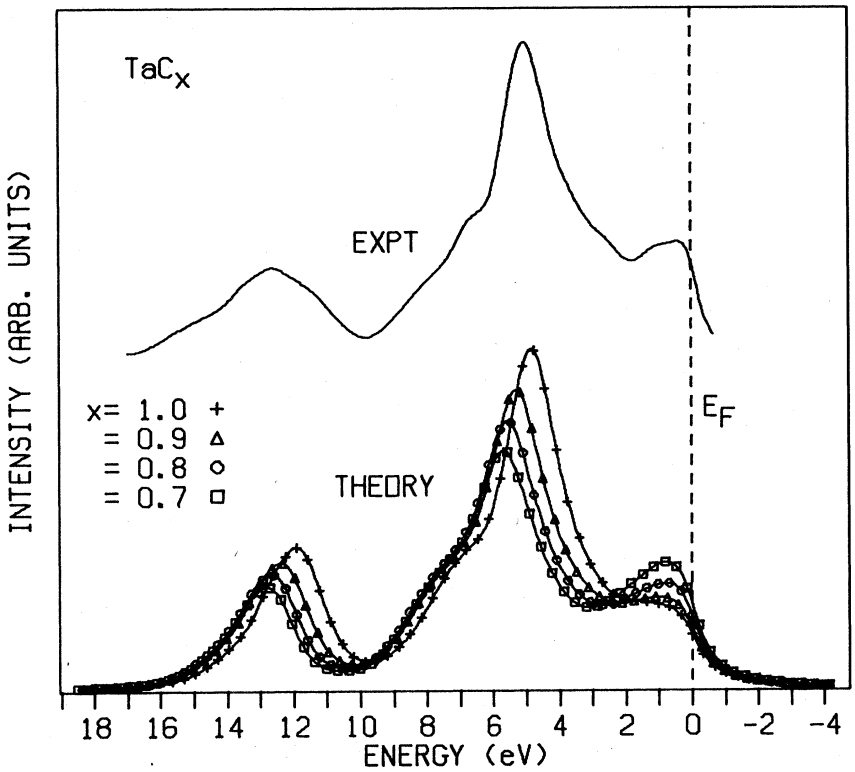

FIG. 14. Experimental photoelectron spectrum of Ref. 28 (top curve), and Lorentzian-broadened total densities of states (γ=1.0 eV FWHM) for TaC_x.

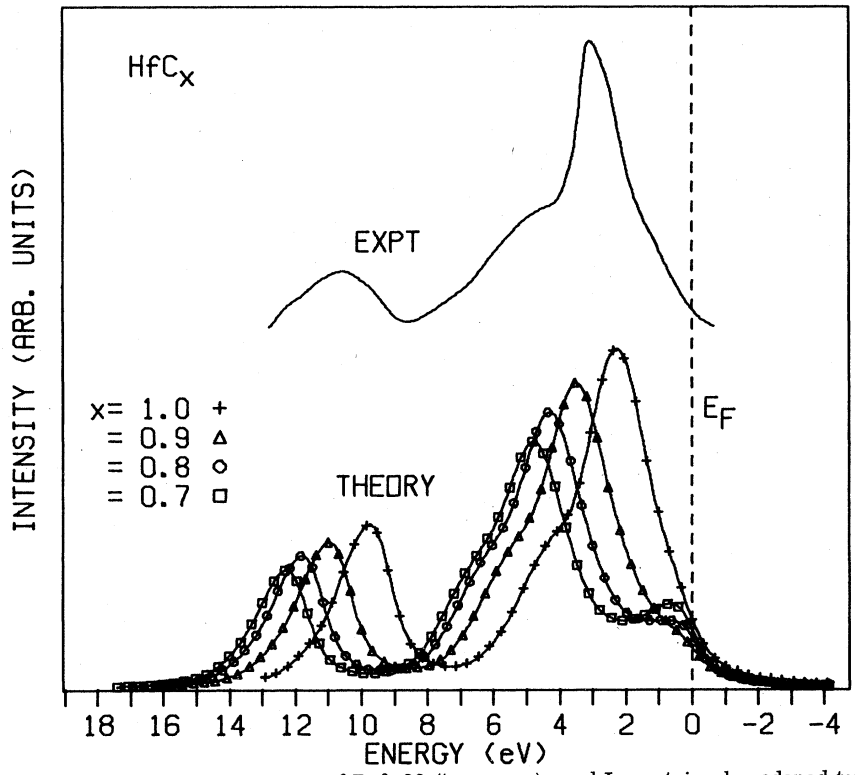

FIG. 15. Experimental photoelectron spectrum of Ref. 28 (top curve), and Lorentzian-broadened total densities of states (γ=1.0 eV FWHM) for HfC_x.

TABLE IV. Peak locations (with respect to the Fermi energy, E_F) of the broadened total density of states and the experimental values from photoelectron measurements. Entries are in eV below E_F. Peaks I, II, and III are the peaks going from the bottom to the top of the valence bands, respectively (see Figs. 13–15).

	NbC_x				TaC_x				HfC_x			
$x\rightarrow$	1.0	0.9	0.8	0.7	1.0	0.9	0.8	0.7	1.0	0.9	0.8	0.7
Peak I	11.6	12.0	12.2	12.3	11.9	12.4	12.6	12.8	9.7	11.0	11.8	12.3
Peak II	4.6	5.0	5.2	5.4	4.8	5.3	5.6	5.7	2.2	3.5	4.3	4.8
Peak III	0.7	1.0	0.7	0.8	1.3	1.0	0.7	0.8	~0.0	0.1	0.8	0.7
		I	II	III								
expt NbC [a]		11.5	4.5	0.7								
expt TaC [b]		12.5	5.2	~1.0								
expt HfC [b]		10.5	3.2	~0.0								

[a] Reference 43.

[b] Reference 28.

unknown. The reason that this is important is that the theoretical peak positions for HfC_x are very sensitive to x owing to the particularly strong x dependence of E_F. The experimental-theoretical agreement for HfC_x would be very good if the HfC_x sample corresponded to $x \sim 0.95$. These remarks also apply, to a lesser extent, to the TaC_x comparison. Further support for our theoretical results comes from the excellent agreement with the measured peak I-peak II separations for all three carbides (this separation is independent of the uncertainty in determining the position of E_F from the experimental data).

We finally call attention to the variations in shape and height of the peak at ~0.5 eV below E_F for the different x values. In all cases this peak grows substantially (compared with the other two peaks) as x is decreased. This is caused by E_F moving into a region of greater $n(E)$ as the number of carbon vacancies increases. Klima[10] noted the same effect (for the same reason) in the calculated L-emission spectrum of TiC_x. We urge that photoelectron-spectra experiments be performed on a well-characterized series of samples with different values of x so that our theoretical predictions of the variation of such spectra with x, and our CPA results in general, may be checked.

X. COMPARISON WITH OTHER EXPERIMENTS

Hall-coefficient measurements for TaC_x have been performed by Santoro and Dolloff,[44] for up to 20% carbon vacancies. The data show a monotonic drop in the Hall coefficient R_0 as the number of carbon vacancies increases. This drop is ~50% between $x = 1.0$ and 0.8. Since R_0 is inversely proportional to the carrier concentration ($R_0 < 0$, so that the carriers are electrons), these measurements support our results of $n(E_F)$ increasing with the number of carbon vacancies. Room-temperature electrical-resistivity measurements[44,45] for TaC_x over a similar composition range as the Hall measurements show an approximate five-fold increase for 20% carbon vacancies compared to stoichiometry. These results are also consistent with the x dependence of $n(E_F)$ that we have calculated (see Ref. 1, p. 186).

Specific-heat measurements have been done over a broad carbon-composition range for both NbC_x and TaC_x.[46] Although the experimental measurements by different groups using samples having the same nominal carbon compositions show large differences for the low-temperature electronic contribution γT, the general trend is that γ decreases with increasing carbon vacancies. It can be shown that $\gamma \propto n(E_F)(1+\lambda)$ for stoichiometric materials. Although we find that our theoretical values of $n(E_F)$ increase with carbon vacancies (opposite to γ), it is also true that λ must decrease due to the vanishing of superconductivity for $x \approx 0.8$, as we have discussed in Sec. XIII. Empirical estimates of $\lambda(x)$ [by inverting the T_c Eq. (11)], together with our calculated values of $n(E_F, x)$ do not show the rapid drop of γ with decreasing x that is observed for NbC_x and TaC_x. However unusual phonon effects due to carbon vacancies, or electron-lifetime effects due to the vacancies, may give anomalous contributions to the specific heat, omitted in the simplified interpretations. Anomalous phonon contributions to the specific heat of nearly stoichiometric NbC_x and TaC_x have already been proposed by Roedhammer *et al.*[47,48] to explain their specific-heat data.

XI. CONCLUSIONS

In this work we have used the LCAO–CPA approach to study the effects of carbon vacancies in three of the refractory monocarbides. We have shown that charge transfer $M \rightarrow C$ has a great influence on the bonding in these materials and must be considered carefully in interpreting the numerical results or predicting Fermi-level motion. We have pointed out that lifetime-broaden-

ing effects of the electron quasiparticles are important for obtaining a full understanding of the superconducting behavior of these materials. Additional theoretical formulations are needed in this regard. These lifetime effects are also manifest in the substoichiometric Fermi surfaces and should be observable by positron annihilation or Compton scattering measurements. Broadened densities of states compare favorably with photoelectron-spectra measurements if the effects due to carbon vacancies are taken into account. Finally we believe that this work has demonstrated the viability of the LCAO–CPA method in relatively complex systems; further work is in progress to extend the method to handle substitutions and vacancies of transition-metal atoms where the additional complication of d electrons are present.

ACKNOWLEDGMENTS

We thank J. S. Faulkner for discussions regarding extending the LCAO–CPA method to include p states of the vacancy atom; L. S. Birks for discussions of bonding in the carbides; W. Temmerman for discussions regarding interpretations of the lifetime-broadened Fermi surfaces; and J. H. Weaver for his NbC photoelectron-spectra data prior to publication.

[1]L. E. Toth, *Transition Metal Carbides and Nitrides* (Academic, New York, 1971).
[2]B. M. Klein and D. A. Papaconstantopoulos, Phys. Rev. Lett. 32, 1193 (1974).
[3]H. G. Smith and W. Gläser, Phys. Rev. Lett. 25, 1611 (1970); H. G. Smith, in *Superconductivity in d- and f-Band Metals*, edited by D. H. Douglass (AIP, New York, 1972).
[4]W. Weber, H. Bilz, and U. Schröder, Phys. Rev. Lett. 28, 600 (1972).
[5]W. Weber, Phys. Rev. B 8, 5082 (1973).
[6]M. Gupta and A. J. Freeman, Phys. Lett. 57A, 291 (1976); Phys. Rev. Lett. 37, 364 (1976); Phys. Rev. B 14, 5205 (1976); in *Superconductivity in d- and f-Band Metals*, edited by D. H. Douglass (Plenum, New York, 1976).
[7]B. M. Klein, L. L. Boyer, and D. A. Papaconstantopoulos, Solid State Commun. 20, 937 (1976).
[8]B. M. Klein, D. A. Papaconstantopoulos, and L. L. Boyer, in *Superconductivity in d- and f-Band Metals*, edited by D. H. Douglass (Plenum, New York, 1976).
[9]J. S. Faulkner, Phys. Rev. B 13, 2391 (1976).
[10]J. Klima, J. Phys. C 12, 3691 (1979).
[11]L. F. Mattheiss, J. H. Wood, and A. C. Switendick, in *Methods in Computational Physics*, edited by B. Alder, S. Fernbach, and M. Rotenberg (Academic, New York, 1968), Vol. 8.
[12]J. O. Dimmock, Solid State Phys. 26, 103 (1971).
[13]K. Schwarz, Phys. Rev. B 5, 2466 (1972).
[14]P. Herzig, Ph.D. thesis, University of Vienna (unpublished).
[15]H. Trebin and H. Bross, J. Phys. C 8, 1181 (1975).
[16]L. F. Mattheiss, Phys. Rev. 151, 450 (1966).
[17]L. L. Boyer and B. M. Klein, Int. J. Quantum Chem. S9, 511 (1975).
[18]D. D. Koelling and B. N. Harmon, J. Phys. C 10, 3107 (1977).
[19]K. Schwarz, J. Phys. C 10, 195 (1977).
[20]P. Weinberger, R. Podloucky, C. P. Mallet, and A. Neckel, J. Phys. C 12, 801 (1979).
[21]D. A. Liberman, D. T. Cromer, and J. T. Waber, Comput. Phys. Commun. 2, 107 (1971).
[22]D. A. Papaconstantopoulos and W. R. Slaughter, Comput. Phys. Commun. 7, 207 (1974); 13, 225 (1977).
[23]G. Lehmann, P. Rennert, M. Taut, and H. Wonn, Phys. Status Solidi 37, K27 (1970); G. Lehmann and M. Taut, Phys. Status Solidi 54, 469 (1972).
[24]J. C. Slater and G. F. Koster, Phys. Rev. 94, 1498 (1954).
[25]D. A. Papaconstantopoulos, B. M. Klein, J. S. Faulkner, and L. L. Boyer, Phys. Rev. B 18, 2784 (1978). Band-structure results for $PdH_{1.0}$ and a rigid-band discussion of PdH_x and PdD_x may be found in: D. A. Papaconstantopoulos, B. M. Klein, E. N. Economou, and L. L. Boyer, Phys. Rev. B 17, 141 (1978).
[26]We acknowledge helpful communications from J. S. Faulkner in developing these extensions.
[27]R. W. Simpson, M. S. thesis, University of Florida, 1969 (unpublished).
[28]M. Ihara, M. Hirabayashi, and H. Nakagawa, Phys. Rev. B 14, 1707 (1976).
[29]D. J. Chadi and M. L. Cohen, Phys. Rev. B 10, 496 (1974).
[30]V. I. Potoracha, V. A. Tskhai, and P. V. Geld, Phys. Status Solidi B 48, 119 (1971).
[31]F. M. Mueller, J. W. Garland, M. H. Cohen, and K. H. Bennemann, Ann. Phys. (N.Y.) 67, 19 (1971). The $n(E)$ results using tetrahedral integration are nearly identical.
[32]G. Kamm (private communication).
[33]L. Ramqvist, J. Appl. Phys. 42, 2113 (1971).
[34]For a general discussion of charge transfer see, R. E. Watson, in *Charge Transfer/Electronic Structure of Alloys*, edited by L. H. Bennett and R. H. Willens (Metallurgical Society of the American Institute of Mining, Metallurgical, and Petroleum Engineers, New York, 1974).
[35]C. M. Varma and W. Weber, Phys. Rev. B 19, 6142 (1979).
[36]B. Splettstoßer, Z. Phys. B26, 151 (1977).
[37]W. L. McMillan, Phys. Rev. 167, 331 (1968); P. B. Allen and R. C. Dynes, Phys. Rev. B 12, 905 (1975).
[38]B. M. Klein and D. A. Papaconstantopoulos, J. Phys. F 6, 1135 (1976).
[39]G. D. Gaspari and B. L. Gyorffy, Phys. Rev. Lett. 28, 801 (1972).

[40]B. M. Klein, D. A. Papaconstantopoulos, and L. L. Boyer, presented at the Symposium on Theory of Alloy Phase Formation, 1979, AIME Annual Meeting [J. Met. 31, 56 (1979)], and in *Theory of Alloy Phase Formation*, edited by L. H. Bennett (Metallurgical Society of the American Institute of Mining, Metallurgical, and Petroleum Engineers, New York, in press).
[41]G. Ries and H. Winter, J. Phys. F 10, 1 (1980).
[42]K. Schwarz and N. Rösch, J. Phys. C 9, L433 (1976).
[43]J. H. Weaver and F. A. Schmidt, Phys. Lett. 77A, 73 (1980).
[44]G. Santoro and R. T. Dolloff, J. Appl. Phys. 39, 2293 (1968).
[45]J. R. Cooper and R. L. Hansler, J. Chem. Phys. 39, 248 (1963).
[46]See, Ref. 1, Chaps. 4 and 6 for a discussion of the specific-heat experiments including a number of references.
[47]P. Roedhammer, E. Gmelin, and W. Weber, Solid State Commun. 16, 1205 (1975).
[48]P. Roedhammer, W. Weber, E. Gmelin, and K. H. Rieder, J. Chem. Phys. 64, 581 (1976).